

Communication

Open Access



Thin-walled hollow fibers for flexible high energy density fiber-shaped supercapacitors

Chuan He^{1,2}, Jianli Cheng¹, Yuhang Liu¹, Xicui Zhang³, Bin Wang^{1,2}

¹Institute of Chemical Materials, China Academy of Engineering Physics, Mianyang 621900, Sichuan, China.

²Institute of Fundamental and Frontier Sciences, Yangtze Delta Region Institute (Huzhou), University of Electronic Sciences and Technology of China, Chengdu 611731, Sichuan, China.

³Sichuan Institute of Product Quality Supervision & Inspection, Chengdu 610100, Sichuan, China.

Correspondence to: Prof. Xicui Zhang, Sichuan Institute of Product Quality Supervision & Inspection, No.16 XingMao Street, Chengdu 610100, Sichuan, China. E-mail: zhangxicui216@163.com; Prof. Bin Wang, Institute of Fundamental and Frontier Sciences, Yangtze Delta Region Institute (Huzhou), University of Electronic Sciences and Technology of China, No. 2006 Xiyuan Avenue, Chengdu 611731, Sichuan, China. E-mail: binwang@uestc.edu.cn

How to cite this article: He C, Cheng J, Liu Y, Zhang X, Wang B. Thin-walled hollow fibers for flexible high energy density fiber-shaped supercapacitors. *Energy Mater* 2021;1:100010. <https://dx.doi.org/10.20517/energymater.2021.14>

Received: 23 Sep 2021 **First Decision:** 18 Oct 2021 **Revised:** 25 Oct 2021 **Accepted:** 26 Oct 2021 **Published:** 30 Oct 2021

Academic Editors: Yuping Wu, Jia-Qi Huang **Copy Editor:** Yue-Yue Zhang **Production Editor:** Yue-Yue Zhang

Abstract

Fiber-shaped supercapacitors, which occupy minimal volume and possess remarkable flexibility, are particularly promising candidates for next-generation smart wearable devices. However, the state-of-the-art energy density and mechanical properties of fiber-shaped electrodes are far from satisfactory. Herein, hollow poly(3,4-ethylenedioxythiophene):polystyrene sulfonate thin-walled fibers (HPFs) are continuously prepared by coaxial wet-spinning. These HPFs combine a simple and high continuous preparation with high electrochemical performance and flexibility, owing to their hollow nature, small diameter (125 μm) and thin wall structure (8 μm). As a result, the HPFs display a specific areal capacitance of 115.2 mF cm^{-2} at a current density of 0.3 mA cm^{-2} with a high energy density of 9 $\mu\text{Wh cm}^{-2}$ at a power density of 0.112 mW cm^{-2} . Furthermore, the HPFs maintain 81% of the initial capacitance after 10,000 cycles with ~100% Coulombic efficiency. More importantly, the specific capacitance is almost completely maintained after bending 3000 times at 180°.

Keywords: Fiber-shaped supercapacitors, PEDOT:PSS, energy density, flexible



© The Author(s) 2021. **Open Access** This article is licensed under a Creative Commons Attribution 4.0 International License (<https://creativecommons.org/licenses/by/4.0/>), which permits unrestricted use, sharing, adaptation, distribution and reproduction in any medium or format, for any purpose, even commercially, as long as you give appropriate credit to the original author(s) and the source, provide a link to the Creative Commons license, and indicate if changes were made.



INTRODUCTION

With the emergence of fifth-generation wireless technology, flexible electronic devices and smart textiles hold significant potential for the next technological revolution by providing flexible, integrated and diverse applications in areas such as emergency and health management, smart homes and surveillance^[1-4]. Among the different components of wearable devices, energy storage devices, such as supercapacitors, are one of the vital components and they need to meet the flexibility, wearability and high electrochemical performance requirements for application in flexible electronic devices. Traditional energy storage devices, such as symmetrical capacitors and supercapacitors, play an important role in human daily life. However, they cannot meet the flexibility and wearability demands of flexible electronic devices, owing to their intrinsically stiff structure^[5,6].

Inspired by textile clothing fibers, fiber-shaped electrodes have become a hot topic because of their intrinsic flexibility, easy integration into textiles and facile preparation^[7-10]. Conductive polymers, such as poly(3,4-ethylenedioxythiophene):polystyrene sulfonate (PEDOT:PSS), can simultaneously combine electrode materials with high conductivity. Furthermore, PEDOT:PSS polymers are also commercially available with outstanding aqueous distribution performance. More importantly, PEDOT:PSS electrodes, with the advantages of fast charge-discharge capability, one-dimensional intrinsic flexibility and superb rate performance^[11], represent ideal alternatives for preparing flexible supercapacitor devices. For example, Yuan prepared meter-long PEDOT:PSS fibers with good mechanical properties. The prepared PEDOT:PSS fibers could be easily woven, sewed, knotted and braided as a fiber-shaped yarn supercapacitor electrode with an areal energy density of $4.13 \mu\text{Wh cm}^{-2}$ and robust performance (strength strain of 85 MPa) under repeated bending tests^[12]. Wang reported a highly crystalline “all-in-one” PEDOT:PSS fiber electrode with a high electrical conductivity of 1771.8 S cm^{-1} and a tensile strength of 112.7 MPa. The assembled eight series-connected supercapacitor groups displayed an energy density of $41.1 \mu\text{Wh cm}^{-2}$ at a power density of 3520 mW cm^{-2} and without significant capacitance degradation after stretching up to 400%^[13]. These works highlight the potential of PEDOT:PSS fiber-shaped electrodes for flexible electronic devices.

Nevertheless, PEDOT:PSS fiber electrodes are known to be solid structures with relatively low capacitance and limited specific energy density, owing to their low effective specific surface area (E-SSA), which refers to the actual electrolyte contact area^[14]. It is well known that the adsorption of electrolyte ions inside solid fibers is very limited, primarily due to the difficulty of ion diffusion along the radial direction of the fiber electrode^[15]. Therefore, efficiently improving the E-SSA of a fiber electrode is one of the most urgent challenges for achieving high energy density. Qu *et al.*^[16] proposed a confined hydrothermal method that depends on the gas released during graphene oxide (GO) reduction to fabricate reduced graphene oxide (rGO)/PEDOT:PSS hollow composite fibers (HCFs). In addition, the areal capacitance of HCFs has a significant improvement of 60% compared to the solid composite fibers because of the hollow interior. However, this method cannot realize continuous preparation because of the limited length of capillary glass tubes. Furthermore, the uniformity of hollow structures requires precise control of the experimental conditions. Therefore, combining simple and high operability continuous wet-spinning with the hollow structure concept may be an effective strategy to improve the energy density and mechanical properties simultaneously.

In this work, thin-walled hollow PEDOT:PSS fiber electrodes with high flexibility and electrical conductivity are prepared by rational design via coaxial wet-spinning. The prepared fiber electrodes show good flexibility with a high tensile strength of 383 MPa at a large breaking strain of 25% and a high electrical conductivity of 362.8 S cm^{-1} (1514 S cm^{-1} calculated by excluding the hollow interior volume). In addition, the fiber electrodes can be rolled up and woven into textiles without any obvious electrochemical performance decay.

When used as electrode materials for gel electrolyte fiber-shaped supercapacitors (FSCs), they show a wide potential window of 0.0–1.5 V and a high energy density of up to $9 \mu\text{Wh cm}^{-2}$ at a power density of 0.112 mW cm^{-2} . Furthermore, the specific capacitance remains relatively unaffected after bending 3000 times and can maintain an initial specific capacitance of 81% after 10000 cycles. This excellent electrochemical performance can be attributed to the unique hollow structure, stable gel electrolyte and unique electrochemical characteristics of the PEDOT:PSS fibers. This work provides an alternative method for the design of flexible FSC systems with promising performance for applications in wearable and flexible electronics.

EXPERIMENTAL

Materials

Clevios PH1000 (PEDOT:PSS, 1.0–1.3 wt.%) was purchased from HC Starck, Inc. Lithium chloride (LiCl, AR), polyvinyl alcohol (PVA, AR) 1788 (Mw 75,000–78,000) and methanol (MeOH, AR) were provided by Aladdin. CaCl_2 (AR) and concentrated H_2SO_4 ($\geq 98\%$) were purchased from Kelong Chemical Reagent Company.

Synthesis of hollow and solid PEDOT:PSS fibers by wet-spinning

The PEDOT:PSS was concentrated at 2.0 wt.% by evaporating water at 50°C . Two microinjection pumps injected the coagulation solution and the concentrated PEDOT:PSS from different syringes into the coagulation solution with CaCl_2 (2.5wt.%) which consists of a water:ethanol solution with a volume ratio of 1:3 at extruded velocities of 3.0 and 1.5 min/mL, respectively. The sizes of the coaxial needles used in the wet-spinning were 18G and 27G. The hollow PEDOT:PSS fibers (HPFs) were fully cross-linked in the coagulation bath for 30 min to maintain their morphology. They were then washed by deionized water and immersed in the MeOH solvent for 30 min to remove the long PSS chains from the surfaces of the fibers. Subsequently, the HPFs were dried on a polytetrafluoroethylene plate at 90°C for 10 min. Finally, the HPFs were immersed in concentrated sulfuric acid within 30 min and sufficiently washed by deionized water to remove part of the insulated PSS. The HPFs were then dried in an oven at 120°C for 10 min to remove the residual water. The preparation conditions for the solid PEDOT:PSS fibers (SPFs) were similar but without pumping of the coagulation bath.

Preparation of gel electrolyte and assembly of gel electrolyte FSCs

First, a 3.5 M LiCl solution was prepared and stirred by a magnetic stirrer until it was completely dissolved. Second, 3 g of PVA were dissolved in a 30 mL LiCl solution at 80°C . Finally, it was continually stirred until the gel solution became clear. For the FSCs, two HPFs or SPFs were placed side by side in parallel and covered with the PVA-LiCl gel electrolyte on the surface. Both ends of the fibers were fixed to the glass slide using conductive tapes and silver adhesives.

Characterization and electrochemical tests

The surface morphologies of the HPFs and SPFs were measured by scanning electron microscopy (SEM, Ultra 55, Carl Zeiss SMT Pte Ltd.). The strain-stress curves of the HPFs and SPFs were measured by a microcomputer controlled electronic universal material testing machine (HY-0350, Shanghai Heng Wing Precision Instrument Co., Ltd.). The Fourier transform infrared spectra were measured at a scanning range from 4000 to 500 cm^{-1} [WQF-530, Beijing Beifen-Ruili Analytical Instrument (Group) Co., Ltd.]. X-ray diffraction (XRD) was measured by a Bruker D2 diffractometer using $\text{Cu K}\alpha$ radiation at a wavelength of 1.5406 \AA . Cyclic voltammetry (CV) with scan rates from 20 to 200 mV s^{-1} and electrochemical impedance spectroscopy (EIS) in a frequency range of 200 kHz to 100 mHz at 0 V bias with an AC amplitude of 10 mV were measured using a VSP-300 electrochemical workstation (Bio-Logic SAS, France). Furthermore, the conductivity of the fiber electrodes was obtained by linear scanning voltammetry (LSV) at a scan rate of 5

mV s⁻¹ in the range of 0-1 V using the VSP-300 electrochemical workstation. Galvanostatic charge-discharge (GCD) curves were recorded by an Arbin Instruments testing system (BT-2000, Arbin) at a current density of 2 mA cm⁻².

RESULTS AND DISCUSSION

In order to compare the morphological differences, different fibers with or without the hollow structure (HPFs and SPFs) were prepared using similar experimental conditions and characterized. [Figure 1A](#) illustrates the fabrication procedure, the microstructure of the hollow coaxial fibers and the charge distribution on the internal and external surfaces. In addition, a continuously hollow HPF with a length of ~0.7 m was prepared by wet-spinning, as shown in [Supplementary Figure 1](#), which demonstrates that the method has the potential for continuous scale preparation. The microscopic morphologies of the HPFs and SPFs were characterized by SEM, as displayed in [Figure 1B-E](#). It can be clearly observed in [Figure 1B](#) that the prepared fibers showed a thin-walled structure with a hollow and uniform structure in the fiber center. The diameter of the HPFs was ~125 μm and the wall thickness was only 8 μm, which depends on the different extruded velocities of the concentrated PEDOT:PSS solution and coagulation bath. Interestingly, the thin-walled hollow structure could be well maintained without structure collapse under solvent and high-temperature treatment, thereby demonstrating desirable structural stability.

In comparison, the cross-sectional structure of the SPFs can also be observed from [Figure 1C](#), which demonstrates the solid structure of the prepared PEDOT:PSS fibers with a diameter of ~100 μm. The diameter of the SPFs was smaller than that of the HPFs. The phenomenon of smaller diameters of the SPFs could be ascribed to two reasons. First, without the internal coagulation bath, the external PEDOT:PSS may lead to self-healing during wet-spinning. Second, the interior solid structure makes a greater contribution to the volume shrinkage of the SPFs during evaporation. Furthermore, the side-view SEM images of the HPFs and SPFs are demonstrated in [Figure 1D](#) and [E](#). The diameter of these conductive fibers was uniform, which illustrates the structural stability of the polymer fibers prepared from coaxial wet-spinning. The morphological differences between the SPFs and HPFs can also be clearly observed. With similar experimental conditions, the HPFs demonstrate relatively smooth surfaces compared to the SPFs, owing to an even multi-step solvent treatment and water evaporation process from the internal and external surfaces simultaneously.

To better understand their mechanical performance, the strain-stress curves of the HPFs and SPFs were characterized, as shown in [Figure 2A](#). Interestingly, the tensile strength of the thin-walled HPFs showed a noticeable increase of 87% to 384 MPa compared with that of the SPFs (205 MPa) under the same strain of 25%. The increased tensile strength of the HPFs may be caused by the relatively complete treatment of H₂SO₄ and the stronger π-π interactions of PEDOT. Therefore, it can be anticipated that the prepared hollow one-dimensional fibrous structure benefits the improvement of the mechanical characteristics and specific capacitance per mass of the fiber electrodes. [Figure 2B](#) shows the LSV curves of the SPFs and HPFs at a scanning rate of 5 mV s⁻¹. The conductivity of the SPFs and HPFs could be calculated by equation (1):

$$\sigma = \frac{L}{RS} \quad (1)$$

where L , R and S are the length, resistance and cross-section area of the fiber electrodes, respectively.

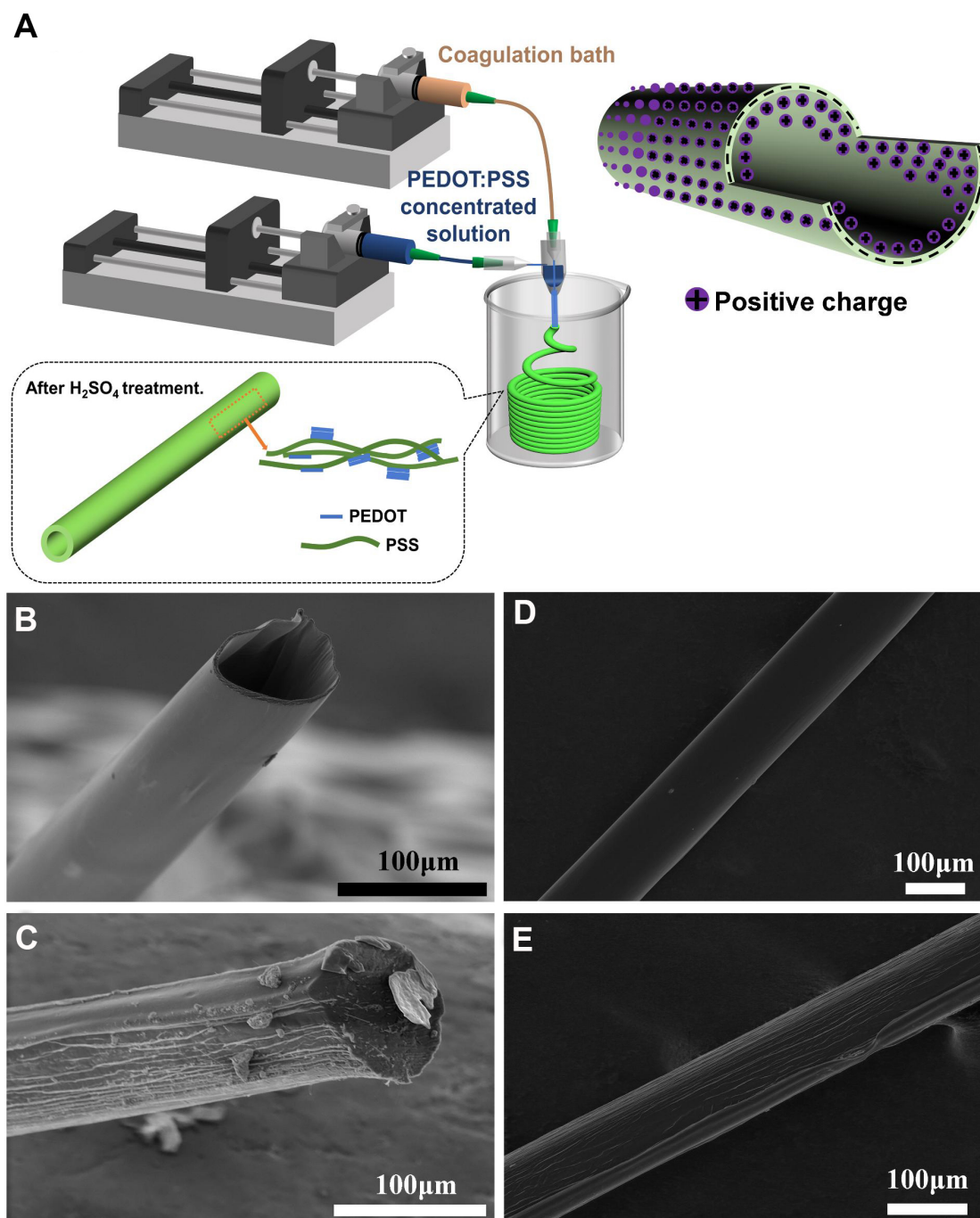


Figure 1. (A) Schematic illustration of preparation process, microstructure and surface charge distribution of HPFs. Cross-sectional SEM images of (B) HPFs and (C) SPFs. Side-view SEM images of (D) HPFs and (E) SPFs. HPF: Hollow poly(3,4-ethylenedioxythiophene):polystyrene sulfonate thin-walled fibers; SPF: solid PEDOT:PSS fibers; SEM: scanning electron microscopy.

The HPFs displayed an electrical conductivity of 1514 S cm^{-1} calculated by excluding the area of the hollow interior. In contrast, the conductivity of the SPFs was 421 S cm^{-1} , which is $\sim 25\%$ that of the HPFs. Moreover, the electrochemical performance of the HPFs and SPFs were also measured by EIS, with the results shown in [Figure 2C](#) for a frequency range of 200 kHz to 100 mHz. In the high-frequency region, the X-intercept of the Nyquist plot represents the equivalent series resistance (ESR), corresponding to the electrolyte

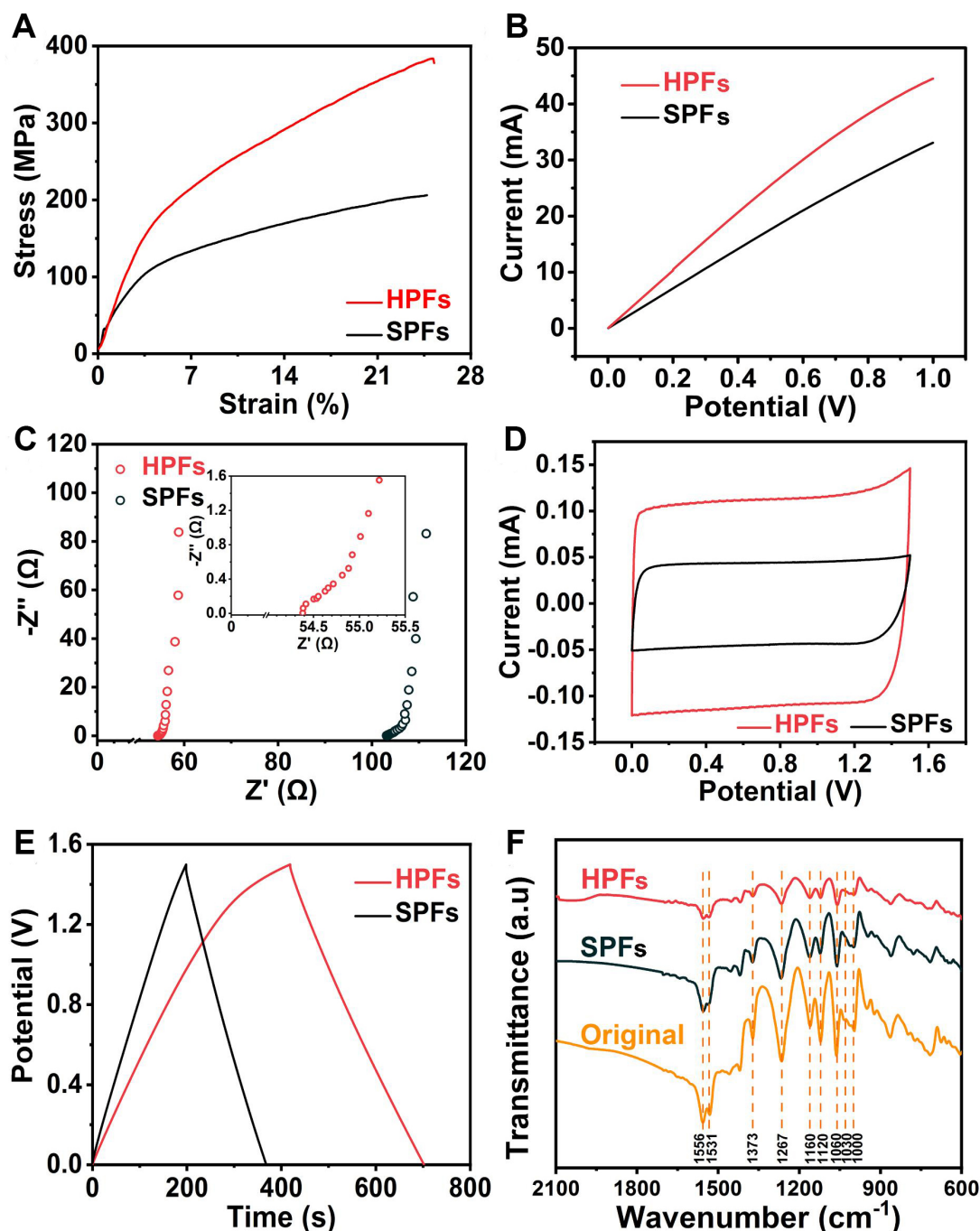


Figure 2. (A) Strain-stress curves of HPFs and SPFs. (B) LSV curves of HPFs and SPFs at a scanning rate of 5 mV s⁻¹. (C) EIS analysis of HPFs and SPFs (inset shows the magnified spectrum of HPFs). (D) CV and (E) GCD curves of HPFs and SPFs at 0.0-1.5 V. (F) Fourier transform infrared spectra of original polymer fibers without H₂SO₄ treatment, SPFs and HPFs. HPF: Hollow poly(3,4-ethylenedioxythiophene):polystyrene sulfonate thin-walled fibers; SPF: solid PEDOT:PSS fibers; LSV: linear scanning voltammetry; EIS: electrochemical impedance spectroscopy; CV: cyclic voltammetry; GCD: galvanostatic charge-discharge.

resistance, internal resistance of the electrode and the contact resistance. The HPF electrode showed a smaller ESR of 54.4 Ω in the high-frequency range in comparison to the ESR of the SPFs (104 Ω). This result may be due to the relative difficulty in removing part of the insulated PSS unit in the solid structure^[17-20]. Obviously, the Nyquist plot shows only one semicircle, corresponding to the charge transfer at the HPF or

SPF electrode/electrolyte interfaces^[21]. Compared with the HPFs, the SPFs displayed a larger semicircle, illustrating that SPFs had a larger charge transfer resistance. These results are in good agreement with the LSV results. In the low-frequency region, the vertical degree of the sloped line showed the corresponding characteristics of pure capacitive behavior. The HPFs showed a more vertical line than the SPFs at low frequency, thereby demonstrating faster ion diffusion.

To further investigate the influence of the hollow structure of the HPFs on their electrochemical properties, the CV and GCD characterization of the assembled FSCs based on HPFs or SPFs was carried out using a 3.5 M PVA-LiCl gel electrolyte in a potential window of 0.0-1.5 V, as shown in Figure 2D and E. The CV curves of the SPFs and HPFs are characterized in Figure 2D with a scanning rate of 20 mV s⁻¹. It can be seen that the area of the rectangular curve for the HPFs was much larger than for the SPFs, demonstrating that the HPFs showed better charge storage capability. Comparing the specific mass capacity (C_m) of the HPFs and SPFs, the C_m of the HPFs (173.8 F g⁻¹) was ~5.4 times higher than that of the SPFs. The specific areal capacitances of the HPFs and SPFs were calculated to be 112.7 and 67.5 mF cm⁻², respectively. Compared to the SPFs, the HPFs exhibited a distinct capacitance increase of ~67%. Furthermore, the discharge times of the HPF and SPF electrodes were 288 and 170 s, respectively. Notably, the GCD curves of the HPF-based FSCs showed a symmetric shape up to 1.5 V with a small IR drop (0.008 V). However, the IR drop of the SPFs was 0.025 V, which was three times that of the HPFs, implying the low conductivity of the SPFs. Therefore, comparing the electrochemical and mechanical test results of the HPFs and SPFs, the HPFs showed higher specific capacitance and better mechanical performance.

This exceptional performance may be derived from the following processes. First, the HSO₄⁻ ions yielded by two H₂SO₄ molecules can partially replace the negatively charged PSS, which is not coupled with PEDOT⁺ according to equation (2):



PEDOT:PSS is then rearranged under the π - π stacking to form dense PEDOT networks with significant morphological and crystalline structure change^[18,22]. Simultaneously, the thin-walled hollow structure of the HPFs facilitates, thorough the solvent treatment and dense conductive network, rapid ion transport and increases the interfacial area of the electrode and electrolytes, leading to increased specific capacitance. To verify this assumption, the attenuated total reflectance-Fourier transform infrared spectroscopy spectra were measured for the SPFs without H₂SO₄ treatment, SPFs and HPFs, as demonstrated in Figure 2F. Several peaks located at 1267, 1373, 1531 and 1556 cm⁻¹ could be attributed to the C-C or C=C stretching of the quinoidal structure and the ring stretching of the thiophene ring of PEDOT:PSS, respectively. The characteristic peaks of -SO₃H in PEDOT:PSS were located at 1060 cm⁻¹ and the absorbance peaks located at 1000, 1030, 1120 and 1160 cm⁻¹ corresponded to the asymmetric and symmetric stretching vibration of the -SO₃⁻ group of the PSS, respectively^[23-25]. Furthermore, compared with that of the pristine SPFs, all of the intensities of these PSS characteristic peaks significantly decreased for the SPFs and HPFs after the sulfuric acid treatment, demonstrating the partial removal of the PSS after treatment.

To characterize the electrochemical properties of the HPFs, the FSCs were prepared by two HPFs placed in parallel using the 3.5 M PVA-LiCl gel electrolyte. Figure 3A shows the CV curves of the HPF electrode measured at different potential windows at a scan rate of 20 mV s⁻¹. It can be observed that there was no obvious polarization when the potential reached 1.5 V. The CV curves maintained their quasi-rectangular shape at 1.5 V, which is consistent with the results of the potential window tested by GCD at a current

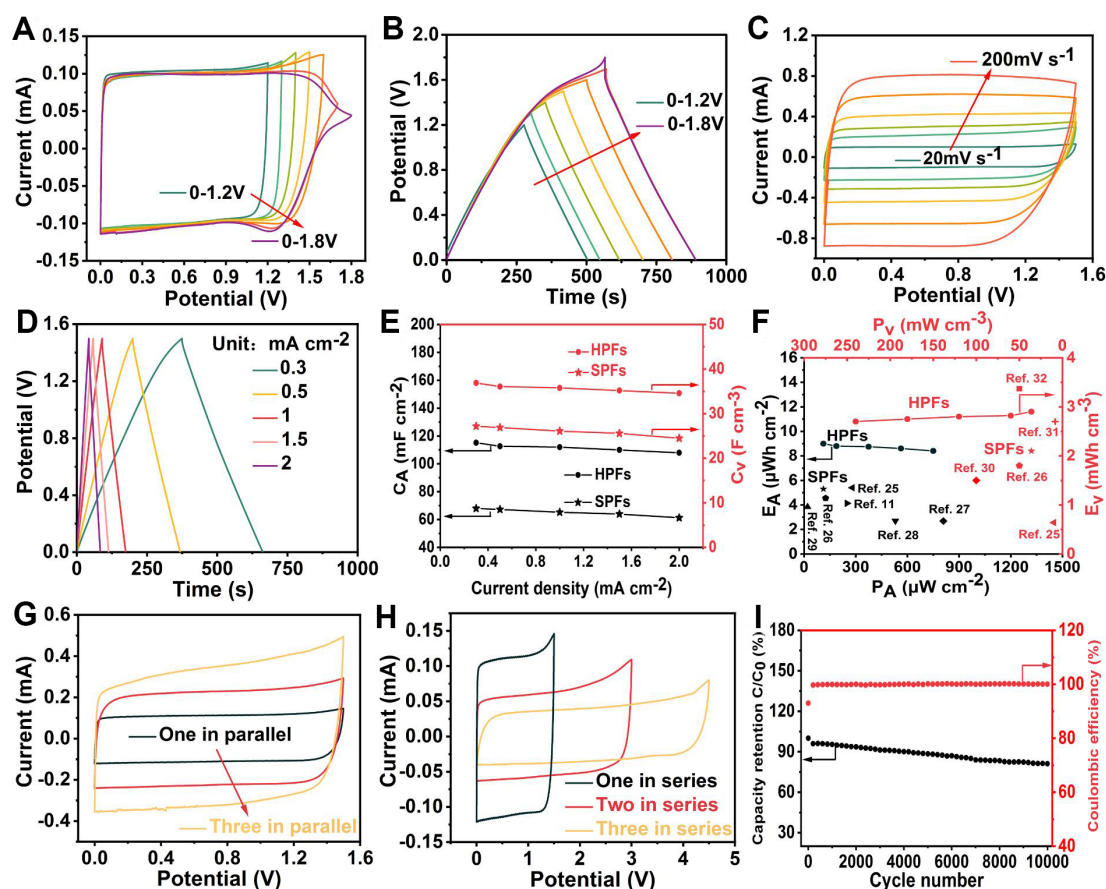


Figure 3. (A) CV and (B) GCD curves of HPFs tested at different potential windows from 0.0 to 1.2–1.8 V. (C) CV curves of HPFs at different scan rates. (D) GCD curves of HPFs at different current densities and (E) rate capabilities of HPFs and SPFs. (F) Ragone plots of HPFs compared with SPFs and other reported results. CV curves of one, two and three devices connected (G) in parallel and (H) in series at a scan rate of 20 mV s⁻¹. (I) Cycling performance of FSCs based on HPFs measured at a current density of 2 mA cm⁻². CV: Cyclic voltammetry; GCD: galvanostatic charge-discharge; HPF: hollow poly(3,4-ethylenedioxythiophene):polystyrene sulfonate thin-walled fibers; FSC: fiber-shaped supercapacitor; SPF: solid PEDOT:PSS fibers.

density of 0.3 mA cm⁻² [Figure 3B]. For potentials of > 1.5 V, the potential polarization increased distinctly. Therefore, the potential window of 0.0–1.5 V was chosen for the subsequent tests of the FSCs. In addition, the CV curves also showed typical rectangular shapes and obviously increased current response values with the scan rate increased from 20 to 200 mV s⁻¹, revealing the fast charge-discharge capability [Figure 3C].

Furthermore, the GCD curves of the HPFs showed outstanding symmetry, as shown in Figure 3D, further verifying the excellent capacitive characteristics. With increasing applied current density, the corresponding discharge time and specific capacitance gradually decreased [Figure 3E]. No obvious IR drop was observed at the beginning process of the constant current discharge, indicative of low internal resistance. Tested at a current density of 0.3 mA cm⁻², the specific areal capacitance of the HPFs reached 115.2 mF cm⁻², corresponding to a mass capacity of 173.8 F g⁻¹ and a volumetric capacitance (C_v) of 36.87 F cm⁻³, while the corresponding values of the SPFs were 68 mF cm⁻², 25.9 F g⁻¹ and 27.2 F cm⁻³, respectively. With the current densities further increased to 1.5 and 2.0 mA cm⁻², the HPFs still maintained high areal capacitances of 110 and 108 mF cm⁻² (35.2 and 34.6 F cm⁻³ for C_v or 169 and 163 F g⁻¹ for C_m), respectively, demonstrating their excellent rate capability and high specific capacitance retention even at very high current densities.

The Ragone plot of the HPF-based FSCs was further calculated, as shown in [Figure 3F](#), to compare the areal energy density (E_A) and volumetric energy density (E_V) with those of the SPF-based FSCs and previously reported fiber-shaped electrodes. In our work, the calculated E_A based on the HPFs was $9 \mu\text{Wh cm}^{-2}$ at a power density of 0.112 mW cm^{-2} , which was higher than for the SPF electrode ($5.3 \mu\text{Wh cm}^{-2}$ and 0.112 mW cm^{-2}), a reported nanoporous gold (NPG)@ MnO_2 hybrid fiber ($5.4 \mu\text{Wh cm}^{-2}$ and 0.28 mW cm^{-2})^[26], a highly-wrinkled rGO-PEDOT:PSS fiber ($4.55 \mu\text{Wh cm}^{-2}$ and 0.125 mW cm^{-2})^[27] and a TiN@C fiber ($2.68 \mu\text{Wh cm}^{-2}$ and 0.809 mW cm^{-2})^[28]. In addition, the E_A found in this study was also better than for asymmetric FSCs supported by carbon fibers coated by MnO_2 (CF/ MnO_2) and MoO_3 (CF/ MoO_3) ($2.7 \mu\text{Wh cm}^{-2}$ and 0.53 mW cm^{-2})^[29], coaxial fibers electrodes with a mixture of rGO and carbon nanotube (CNT) core and sodium carboxymethyl cellulose sheath ($3.84 \mu\text{Wh cm}^{-2}$ and 0.02 mW cm^{-2})^[30] and PEDOT:PSS fibers ($4.13 \mu\text{Wh cm}^{-2}$ and 0.25 mW cm^{-2})^[12]. The HPF-based FSCs delivered an E_V of 2.9 mWh cm^{-3} at a power density of 36 mW cm^{-3} , which exceeded the SPFs (2.1 mWh cm^{-3} and 45 mW cm^{-3}), NPG@ MnO_2 hybrid fibers (0.64 mWh cm^{-3} and 10 mW cm^{-3})^[26], highly-wrinkled rGO-PEDOT:PSS fibers (1.8 mWh cm^{-3} and 50 mW cm^{-3})^[27], asymmetric FSCs fabricated by multi-walled carbon nanotubes with MoS_2 and rGO nanosheets (MWCNT/ MoS_2 -rGO) as anodes and rGO/MWCNTs as cathodes (1.5 mWh cm^{-3} and 100 mW cm^{-3})^[31], MWCNT-PEDOT:PSS hybrid fibers (2.7 mWh cm^{-3} and 8.5 mW cm^{-3})^[32] and is comparable to that of CNT-rGO@ MnO_2 fibers (3.37 mWh cm^{-3} and 50 mW cm^{-3})^[33].

To demonstrate their capability to adapt to the different practical application requirements of devices, different numbers of FSCs based on HPFs were connected in series or parallel, as shown in [Figure 3G](#) and [H](#). The voltage or current of the devices can be increased severalfold with the number of connected devices in series or parallel. As a result, the voltages showed a monotonous linear increase of 1.5, 3.0 and 4.5 V by increasing the number of serial cells from one to three, respectively. Similarly, the current increased with an increased number of parallel-connected devices, demonstrating excellent performance uniformity. Moreover, the long-term cycle stability of the FSCs based on HPFs was evaluated at a current density of 2 mA cm^{-2} . As shown in [Figure 3I](#), the specific capacitance retention after 10,000 cycles was higher than 81%, suggesting that the device exhibited impressive stability over long cycling. More importantly, the Coulombic efficiency was maintained close to 100%, indicating high charge utilization. As shown in [Supplementary Figure 2A](#), the SEM images of the HPFs after cycling do not show an obvious change of the surface or hollow structure, illustrating their good structural stability during long-term cycling. Furthermore, the HPFs after cycling showed a similar pattern with a slight decrease in the XRD intensity [[Supplementary Figure 2B](#)], further verifying their stability. The crystalline decline can be associated with the increased ESR and charge transfer resistance (R_{ct}) shown in [Supplementary Figure 2C](#).

To meet the demands of practical applications, the leakage currents of the HPF- and SPF-based FSCs were analyzed by chronoamperometry at a potential of 1.5 V for 2500 s. Surprisingly, the HPF-based FSCs showed an extremely low leakage current of $2.7 \mu\text{A}$, which demonstrates their stability of electrochemical energy storage compared with the $5.8 \mu\text{A}$ for the SPFs [[Supplementary Figure 3A](#)]. On the basis of the electrical double layer capacitance, the ions are inclined to diffuse into the electrolyte and adsorb on the surface of the fiber electrode because of the voltage and concentration differences between the electrode and electrolyte in the open circuit state. Furthermore, we performed self-discharge tests of the devices by charging them to a certain potential (1.5 V) and then the retained potentials were tested after a long period of rest of 10 h [[Supplementary Figure 3B](#)]. The HPF-based FSCs revealed a better anti-self-discharge property with an open-circuit voltage of 0.68 V, owing to the hollow structure and low leakage current.

To demonstrate their application in flexible electronics, the HPF-based FSCs with a length of $\sim 4 \text{ cm}$ were assembled in a heat shrink tube and filled with a LiCl/PVA gel electrolyte, as shown in [Figure 4A](#). [Figure 4B](#)

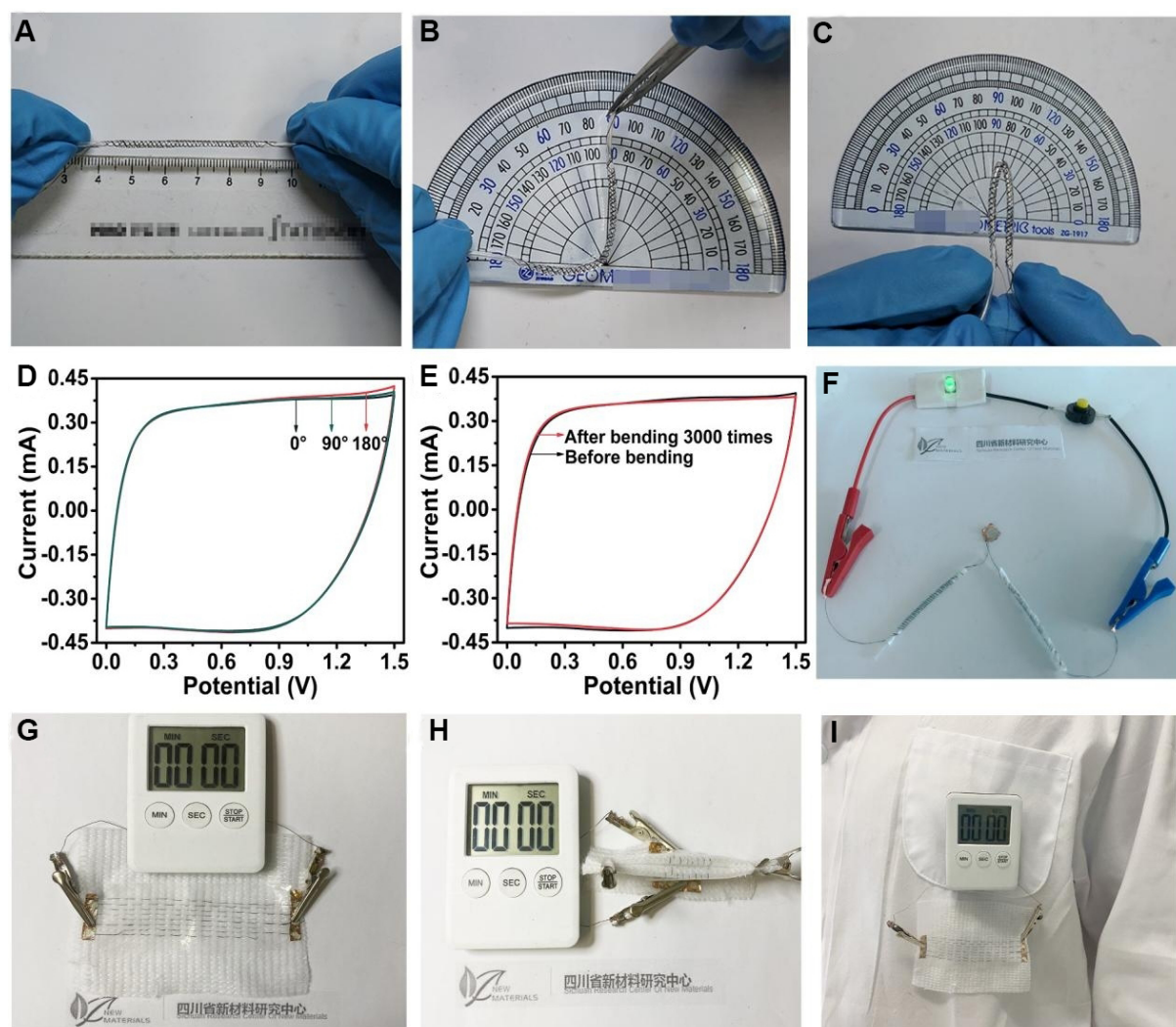


Figure 4. Photographs of HPF-based FSCs of ~4 cm in length at the (A) straight and bent at (B) 90° and (C) 180° states. (D) CV curves of the FSCs bent at different angles at a scan rate of 20 mV s^{-1} . (E) CV curves of FSCs before and after bending at 180° for 3000 times. (F) Optical image of two individual FSCs based on HPF electrodes connected in series to light up a green LED. Fabricated textile devices integrated into the cloth with four HPFs connected in parallel to power an electronic timer at the (G) flat and (H) bending 180° states. (I) Demonstration of a flexible wearable device. HPF: Hollow poly(3,4-ethylenedioxythiophene):polystyrene sulfonate thin-walled fibers; FSC: fiber-shaped supercapacitor; CV: cyclic voltammetry.

-D present the CV curves tested at various bending angles, which are well overlapped without a significant shape change, indicating good adaptability to bend at different angles. More importantly, the assembled device was bent at 180° for 3000 times and the corresponding CV characterized. It can be observed from the CV, as shown in Figure 4E, that the curves do not show a significant change after bending 3000 times, manifesting excellent electrode stability. Additionally, two individual devices connected in series after easily charging could power a green light-emitting diode with a minimum voltage requirement of 2 V for ~8 min [Figure 4F]. Benefiting from the superb mechanical properties of the HPFs, textile supercapacitors were assembled by weaving them into a fabric consisting of four FSCs connected in parallel with a length of 7 cm [Figure 4G], which can directly power a commercial electronic timer with a voltage demand of 1.5 V for 3 min. The demonstrated textile supercapacitor can normally provide the power even with bending at 180° for several times without an obvious performance decay, as shown in Figure 4H and I. The above results

give an encouraging demonstration of these textile supercapacitor devices applied in flexible electronic devices.

CONCLUSION

In summary, hollow thin-walled PEDOT:PSS fiber electrodes with high conductivity, excellent electrochemical performance and good flexibility were prepared by wet-spinning and used as flexible electrodes to assemble high energy density FSCs and textile supercapacitors. By combining the flexibility and specific hollow structure, the HPF-based FSCs showed superb rate capability, high specific capacitance, impressive long-term cycle stability and high capacitance retention after bending 3000 times. Additionally, this exceptional performance may be attributed to the synergistic effects of the unique hollow structure, efficient PEDOT conduction network, wide electrochemical windows and increased contact areas with the electrolyte. In brief, this work provides insights into the potential application of wearable textile supercapacitor devices in flexible electronic devices.

DECLARATIONS

Authors' contributions

Wrote and reviewed the manuscript: He C, Cheng J, Liu Y, Zhang X, Wang B

Availability of data and materials

The linked data has been added in the manuscript. The raw/processed data required to reproduce these findings can be obtained from the request or the first author.

Financial support and sponsorship

The authors acknowledge the financial supports by the National Natural Science Foundation of China (No. 21875226, 52072352, U20A2072), the Foundation for the Youth S&T Innovation Team of Sichuan Province(2020JDTD0035), Tianfu Rencai Plan, the Chengdu Talent plan, and Science and Technology Projects for Administration for Market Regulation of Sichuan Province (SCSJ2020016).

Conflicts of interest

All authors declared that there are no conflicts of interest.

Ethical approval and consent to participate

Not applicable.

Consent for publication

Not applicable.

Copyright

© The Author(s) 2021.

REFERENCES

1. Pan Z, Yang J, Zhang Y, Gao X, Wang J. Quasi-solid-state fiber-shaped aqueous energy storage devices: recent advances and prospects. *J Mater Chem A* 2020;8:6406-33. [DOI](#)
2. Wang L, Fu X, He J, et al. Application challenges in fiber and textile electronics. *Adv Mater* 2020;32:e1901971. [DOI](#) [PubMed](#)
3. Manjakkal L, Pullanchiyodan A, Yogeswaran N, Hosseini ES, Dahiya R. A wearable supercapacitor based on conductive PEDOT:PSS-coated cloth and a sweat electrolyte. *Adv Mater* 2020;32:e1907254. [DOI](#) [PubMed](#)
4. Lai Y, Lu H, Wu H, et al. Elastic multifunctional liquid-metal fibers for harvesting mechanical and electromagnetic energy and as self-powered sensors. *Adv Energy Mater* 2021;11:2100411. [DOI](#)
5. Yang J, Li G, Pan Z, et al. All-solid-state high-energy asymmetric supercapacitors enabled by three-dimensional mixed-valent MnOx nanospire and graphene electrodes. *ACS Appl Mater Interfaces* 2015;7:22172-80. [DOI](#) [PubMed](#)
6. Zhu M, Wang Z, Li H, et al. Light-permeable, photoluminescent microbatteries embedded in the color filter of a screen. *Energy*

- Environ Sci* 2018;11:2414-22. DOI
7. Ma W, Zhang Y, Pan S, et al. Smart fibers for energy conversion and storage. *Chem Soc Rev* 2021;50:7009-61. DOI PubMed
 8. Lee C, Lai K, Lin C, et al. A paper-based electrode using a graphene dot/PEDOT:PSS composite for flexible solar cells. *Nano Energy* 2017;36:260-7. DOI
 9. Song W, Fan X, Xu B, et al. All-solution-processed metal-oxide-free flexible organic solar cells with over 10% efficiency. *Adv Mater* 2018;30:e1800075. DOI PubMed
 10. Tian J, Cui N, Chen P, Guo K, Chen X. High-performance wearable supercapacitors based on PANI/N-CNT@CNT fiber with a designed hierarchical core-sheath structure. *J Mater Chem A* 2021;9:20635-44. DOI
 11. Yang Z, Jia Y, Niu Y, et al. One-step wet-spinning assembly of twisting-structured graphene/carbon nanotube fiber supercapacitor. *Journal of Energy Chemistry* 2020;51:434-41. DOI
 12. Yuan D, Li B, Cheng J, et al. Twisted yarns for fiber-shaped supercapacitors based on wet-spun PEDOT:PSS fibers from aqueous coagulation. *J Mater Chem A* 2016;4:11616-24. DOI
 13. Wang Z, Cheng J, Guan Q, et al. All-in-one fiber for stretchable fiber-shaped tandem supercapacitors. *Nano Energy* 2018;45:210-9. DOI
 14. Zhang L, Yang X, Zhang F, et al. Controlling the effective surface area and pore size distribution of sp² carbon materials and their impact on the capacitance performance of these materials. *J Am Chem Soc* 2013;135:5921-9. DOI PubMed
 15. Ma W, Li W, Li M, et al. Unzipped carbon nanotube/graphene hybrid fiber with less “dead volume” for ultrahigh volumetric energy density supercapacitors. *Adv Funct Mater* 2021;31:2100195. DOI
 16. Qu G, Cheng J, Li X, et al. A fiber supercapacitor with high energy density based on hollow graphene/conducting polymer fiber electrode. *Adv Mater* 2016;28:3646-52. DOI PubMed
 17. Jalili R, Razal JM, Innis PC, Wallace GG. One-step wet-spinning process of poly(3,4-ethylenedioxythiophene):poly(styrenesulfonate) fibers and the origin of higher electrical conductivity. *Adv Funct Mater* 2011;21:3363-70. DOI
 18. Kim N, Kee S, Lee SH, et al. Highly conductive PEDOT:PSS nanofibrils induced by solution-processed crystallization. *Adv Mater* 2014;26:2268-72, 2109. DOI PubMed
 19. Lang U, Müller E, Naujoks N, Dual J. Microscopical Investigations of PEDOT:PSS thin films. *Adv Funct Mater* 2009;19:1215-20. DOI
 20. Vosgueritchian M, Lipomi DJ, Bao Z. Highly conductive and transparent PEDOT:PSS films with a fluorosurfactant for stretchable and flexible transparent electrodes. *Adv Funct Mater* 2012;22:421-8. DOI
 21. Cai S, Huang T, Chen H, Salman M, Gopalsamy K, Gao C. Wet-spinning of ternary synergistic coaxial fibers for high performance yarn supercapacitors. *J Mater Chem A* 2017;5:22489-94. DOI
 22. Xu D, Shen H, Wang W, et al. Effect of H₂SO₄ solution treatment on adhesion, charge transfer, and catalytic performance of screen-printed PEDOT:PSS. *Chemphyschem* 2019;20:374-82. DOI
 23. Li Y, Ren G, Zhang Z, et al. A strong and highly flexible aramid nanofibers/PEDOT:PSS film for all-solid-state supercapacitors with superior cycling stability. *J Mater Chem A* 2016;4:17324-32. DOI
 24. Alemu D, Wei H, Ho K, Chu C. Highly conductive PEDOT:PSS electrode by simple film treatment with methanol for ITO-free polymer solar cells. *Energy Environ Sci* 2012;5:9662. DOI
 25. Xu T, Yang D, Zhang S, Zhao T, Zhang M, Yu Z. Antifreezing and stretchable all-gel-state supercapacitor with enhanced capacitances established by graphene/PEDOT-polyvinyl alcohol hydrogel fibers with dual networks. *Carbon* 2021;171:201-10. DOI
 26. Xu H, Hu X, Sun Y, Yang H, Liu X, Huang Y. Flexible fiber-shaped supercapacitors based on hierarchically nanostructured composite electrodes. *Nano Res* 2015;8:1148-58. DOI
 27. Li B, Cheng J, Wang Z, Li Y, Ni W, Wang B. Highly-wrinkled reduced graphene oxide-conductive polymer fibers for flexible fiber-shaped and interdigital-designed supercapacitors. *J Power Sources* 2018;376:117-24. DOI
 28. Sun P, Lin R, Wang Z, et al. Rational design of carbon shell endows TiN@C nanotube based fiber supercapacitors with significantly enhanced mechanical stability and electrochemical performance. *Nano Energy* 2017;31:432-40. DOI
 29. Noh J, Yoon C, Kim YK, Jang J. High performance asymmetric supercapacitor twisted from carbon fiber/MnO₂ and carbon fiber/MoO₃. *Carbon* 2017;116:470-8. DOI
 30. Kou L, Huang T, Zheng B, et al. Coaxial wet-spun yarn supercapacitors for high-energy density and safe wearable electronics. *Nat Commun* 2014;5:3754. DOI PubMed PMC
 31. Sun G, Zhang X, Lin R, Yang J, Zhang H, Chen P. Hybrid fibers made of molybdenum disulfide, reduced graphene oxide, and multi-walled carbon nanotubes for solid-state, flexible, asymmetric supercapacitors. *Angew Chem Int Ed Engl* 2015;54:4651-6. DOI PubMed
 32. Meng C, Qian Y, He J, Dong X. Wet-spinning fabrication of multi-walled carbon nanotubes reinforced poly(3,4-ethylenedioxythiophene)-poly(styrenesulfonate) hybrid fibers for high-performance fiber-shaped supercapacitor. *J Mater Sci: Mater Electron* 2020;31:19293-308. DOI
 33. Wang H, Wang C, Jian M, et al. Superelastic wire-shaped supercapacitor sustaining 850% tensile strain based on carbon nanotube@graphene fiber. *Nano Res* 2018;11:2347-56. DOI